Revista de Metalurgia
April–June 2018, 54 (2), e118
ISSN-L: 0034-8570
https://doi.org/10.3989/revmetalm.118

Microstructural optimization of unalloyed ductile cast irons with a ferritic matrix used in the manufacture of wind turbine rotors

Juan Asensio-Lozano[a], José F. Álvarez-Antolín[b,✉], Carlos H. Álvarez-Pérez[b]

[a]Departamento de Ciencia de los Materiales e Ingeniería Metalúrgica, Escuela de Ingeniería de Minas, Energía y Materiales, Universidad de Oviedo, c/ Independencia 13, 33004 Oviedo, España
[b]Departamento de Ciencia de los Materiales e Ingeniería Metalúrgica, Edificio Departamental Este, Universidad de Oviedo, c/ Wifredo Ricart s/n, 33204 Gijón, España
✉Corresponding author: alvarezflorentino@uniovi.es

Submitted: 15 May 2017; Accepted: 9 December 2017; Available On-line: 14 May 2018

ABSTRACT: The aim of this work was the microstructural optimization of cast irons with nodular graphite for the manufacture of wind turbine hubs, paying preferential attention to the geometry and distribution of graphite spheroids to ensure the required mechanical properties for this application. The target was pursued based upon microstructure-properties correlation, in an environment of great competitiveness and exigency marked by current international standards. The methodology followed consisted of the generation of knowledge from tailor-made industrial castings, followed by the analysis of their microstructures, in order to extract valuable conclusions for the production process through the use of statistical analysis. The approach method employed was a Fractional Design of Experiments (DOE) with 7 factors, 16 experiments and resolution IV. The samples from each experiment were cubes of identical geometry, and designed to match a surface-to-volume module equal to 4 cm (1.57 in) found as the highest values in real hubs of 3 MW power wind turbines. It is concluded that the use of nodulizers with traces of lanthanum favour the reduction of the volume fraction of pearlite, although La has proved not to promote the spherical shape of primary graphite. The negative effect of pre-inoculants containing SiC on the spheroidal morphology of graphite has also been verified, and also that low-Mn bearing scrap favours graphite formation and the reduction of the volume fraction of pearlite, in spite of being a carbide forming element. The whitening effect of Mn was minimized with low carbon equivalent melts.

KEYWORDS: Design of experiments; Ductile iron; Gray iron; Nodulizers; Pearlite; Quantitative metallography; Spheroidal graphite; Wind turbine rotor

Citation/Citar como: Asensio-Lozano, J.; Álvarez-Antolín, J.F.; Álvarez-Pérez, C.H. (2018). "Microstructural optimization of unalloyed ductile cast irons with a ferritic matrix used in the manufacture of wind turbine rotors". *Rev. Metal.* 54(2): e118. https://doi.org/10.3989/revmetalm.118

RESUMEN: *Optimización microestructural de fundiciones grises dúctiles no aleadas, con matriz ferrítica, empleadas en la fabricación de bujes de aerogeneradores.* El objetivo de este trabajo fue la optimización microestructural de fundiciones grises con grafito esferoidal y matriz ferrítica, empleadas en la fabricación de bujes de aerogeneradores, prestando una especial atención a la geometría y distribución de los esferoides de grafito para asegurar el cumplimiento de las propiedades mecánicas requeridas para esta aplicación. En un entorno de gran competitividad y exigencia, marcado por los estándares internacionales que establecen las propiedades mecánicas mínimas que deben cumplir los materiales empleados, el cumplimiento de este objetivo se llevó a cabo correlacionando microestructura y propiedades. Para ello, la metodología de investigación consistió en la generación de conocimiento a partir de coladas industriales "a medida", seguido de un análisis de la microestructura, con el fin de extraer conclusiones importantes, de aplicación práctica en el proceso de fabricación, mediante el

empleo de técnicas estadísticas. La herramienta estadística empleada fue un Diseño de Experimentos Fraccional (DOE), con 7 factores, 16 experimentos y resolución IV. Las muestras empleadas en cada experimento fueron cubos de igual geometría, y con un módulo de masividad de valor 4 cm, el cual se encuentra entre los valores más altos alcanzados en los centros reales de los bujes de aerogeneradores con potencia de 3 MW. Se concluye que el empleo de nodulizantes con trazas de lantano favorece la reducción de la fracción de volumen de perlita, aunque se ha demostrado que la presencia de lantano resulta negativa para promover la morfología esferoidal del grafito primario. A su vez, se ha constatado, sobre la morfología esferoidal del grafito, el efecto negativo del empleo de preinoculantes que contienen SiC, y también que la utilización de chatarra con bajo contenido de Mn favorece la formación de grafito y la reducción de la fracción en volumen de perlita. Se ha comprobado que el efecto "blanqueante" del Mn se ve minimizado con bajos carbonos equivalentes.

PALABRAS CLAVE: Buje de aerogenerador; Diseño de experimentos; Fundición dúctil; Fundición gris; Metalografía cuantitativa; Perlita

ORCID ID: Juan Asensio-Lozano (https://orcid.org/0000-0001-6552-2860); José F. Álvarez-Antolín (https://orcid.org/0000-0003-2447-6575); Carlos H. Álvarez-Pérez (https://orcid.org/0000-0001-9377-2410)

1. INTRODUCTION

The rotor or hub of a wind turbine is the rotating element that holds the blades in position such that the wind energy transforms into a rotating movement when the wind hits the blades. The rotor is connected to a low-speed shaft which, by means of a gear box placed at the opposite end of the primary shaft, enables the increase in the rotational speed which is needed to drive the electric generator.

The component under study was manufactured to comply with Euronorm EN-GJS-400-18-LT standard, which corresponds to a spheroidal graphite cast iron (Mottitschka *et al*., 2012). Wind turbine manufacturing specifications for these parts require a tensile strength of over 370 MPa, total elongation greater than 12%, and values above 10 J in the Charpy test at −20 °C (Asensio-Lozano and Álvarez-Antolín, 2007). These mechanical properties are a result of the microstructure of the material (Pan *et al*., 2012). For this reason, the requirements of these manufacturers include a volume fraction of pearlite lower than 5%, in addition to a spheroidal morphology in the primary graphite (Lacaze *et al*., 2016). Recent studies have shown that factors such as graphite morphology and the number of graphite nodules per unit area have a significant effect on the in-service behaviour of the material, especially its fatigue strength (Shiraki *et al*., 2016).

When nodulizing is performed only with magnesium, the transition process leading to a spheroidal shape from a lamellar flake graphite morphology is continuous. When rare earths are added, however, this transition is more abrupt (Geiger *et al*., 2005). One of these elements usually added is cerium, which is associated with the deleterious effect of reducing the influence of the time between nodulizing and casting, as well as on the ductility of these ductile irons (Bockus and Zaldarys, 2010). Cerium and lanthanum tend to increase the number of graphite "counts" per unit area, producing an increase in the undercooling required for the nucleation of graphite (Onsoien *et al*., 1999; Sheikh and Iqbal, 2007). Lanthanum is assigned an additional advantage; namely that of reducing the presence of possible shrinkage micro-cavities and improving the "sphericity" of small-sized graphite nodules (Pedersen and Tiedje, 2009). The origin of the fracture leading to fatigue failure tends to be located in areas in the vicinity of a graphite nodule whose sphericity has "degenerated", or in areas adjacent to micro-cavities (Shiraki *et al*., 2015). Cracks have been observed to initiate at spherical graphite and carbides even at a small load, and afterwards propagated readily through the adjacent graphite or carbides, thereby resulting in the lowest fracture toughness (Han *et al*., 2013).

The aim of this study is to identify the manufacturing parameters that have a significant effect on these two micro-structural factors (Asensio-Lozano *et al*., 2008). The study was accordingly conducted on specimens with an equivalent volume-to-surface ratio to that of the part under study with the aim of transferring the results of this analysis to the actual wind turbine hubs. The approach method was a Fractional Design of Experiments (DOE) with 7 factors, 16 experiments (Prat *et al*., 1997) and resolution IV (Box *et al*., 2005).

In the present work, the experiments were conducted on an industrial scale and the samples obtained were cubes of 200-mm sides with the same volume-to-surface ratio as for the most controversial regions in 3 MW rotors (Guzel *et al.*, 2014). This ratio was found to be equal to 4 cm (1.57 inches).

From the results obtained, it is concluded that the use of nodulizers with traces of lanthanum helps to reduce the volume fraction of pearlite. However, this nodulization does not promote the formation of spheroidal graphite. Furthermore, it was found that this effect could be counteracted using scrap with

low-Mn content. It was also discovered that using low-Mn melts helps to reduce the fraction of primary pearlite, and that pre-inoculation with SiC has a negative effect on the precipitation of spheroidal graphite.

To corroborate the results, a new cube was melted, placing the factors with a significant effect at their optimum levels. Samples taken from this cube were subjected to metallographic characterization and verification of their mechanical properties (tensile and Charpy tests at −20 °C) to verify that the minimum required values were exceeded.

2. MATERIAL AND METHODS

Table 1 shows the industrial factors selected in the present analysis along with the levels selected for each of them. Table 2 illustrates of the matrix of experiments in the present design. The samples in each experiment were manufactured on an industrial scale using the same melt in the ladle formerly used to cast each hub. Table 3 shows the target chemical composition for each experiment. The effect of Mn was included in the study. Mn is incorporated into the molten bath from steel scrap; and, it has a remarkable effect on the mechanical properties of these ductile cast irons with a ferritic matrix (Asenjo *et al*., 2011).

Table 1. Factors and levels analyzed

Code	Metallurgical Factors	Level −1	Level +1
A	P	0.025%	0.04%
B	Mn	0.1%	0.3%
C	SiC	3 Kg/T	0
D	Casting temperature	1320 °C	1360 °C
E	Carbon equivalent	4.3%	4.5%
F	Post-inoculation	Post-Inoc.−1	Post-Inoc.+1
G	Nodulizer	Nodulizer−1	Nodulizer+1

Table 2. Generated array for the DOE $\left(2_{IV}^{7-3}\right)$ array

No.	A	B	C	D	E	F	G	Generators	Confusions
1	–1	–1	–1	–1	–1	–1	–1		A
2	+1	–1	–1	–1	+1	–1	+1		B
3	–1	+1	–1	–1	+1	+1	–1		C
4	+1	+1	–1	–1	–1	+1	+1		D
5	–1	–1	+1	–1	+1	+1	+1		E
6	+1	–1	+1	–1	–1	+1	–1		F
7	–1	+1	+1	–1	–1	–1	+1		G
8	+1	+1	+1	–1	+1	–1	–1	E=ABC	AB+CE+FG
9	–1	–1	–1	+1	–1	+1	+1	F=BCD	AC+BE+DG
10	+1	–1	–1	+1	+1	+1	–1	G=ACD	AD+CG+EF
11	–1	+1	–1	+1	+1	–1	+1		AF+BG+AG
12	+1	+1	–1	+1	–1	–1	–1		BC+AE+DF
13	–1	–1	+1	+1	+1	–1	–1		BD+CF+EG
14	+1	–1	+1	+1	–1	–1	+1		CD+BF+AG
15	–1	+1	+1	+1	–1	+1	–1		ABD
16	+1	+1	+1	+1	+1	+1	+1		

Pre-inoculation or ladle inoculation and nodulizing processes were performed simultaneously on pouring the molten metal from the furnace to the ladle. This was achieved by placing FeSiMg containing alloys in a compartment made with refractory bricks in the bottom ladle covered by a thin steel plate. This helps to retard the violent reaction in the melt when the molten metal contacts the Mg bearing alloys (Skjegstad and Skaland, 1996). The reaction of Si and Mg, apart from remaining in liquid solution, also helps to deoxidize and desulfurize the melt creating a floating slag consisting mainly of silicates, oxides and sulphides, which must be removed to avoid dross entrapment in the casting by slag carryover during casting. The process is followed by tundish post-inoculation which allows enough time for complex Si-bearing alloys to melt, and secondary slag flotation and retention while the clean treated metal flows down through the sprue to the runners and then into the mould.

Table 4 shows the chemical composition of the alloys used. It should be noted that the level +1 of this factor includes traces of lanthanum. To improve the inoculation yield, a second inoculation process is conducted at a low temperature, at the time of casting.

Table 5 shows the basic chemistry of the post-inoculants used. The post-inoculant used for level −1, was deposited on the pouring tundish located atop the mould. However, the post-inoculant used at level +1 was added directly to the molten stream on pouring the molten iron from the ladle to the tundish during casting (Soivio and Elmquist, 2013).

SiC is added to the furnace to promote molten metal deoxidation in the melting furnace for melt conditioning, bath recarburizing and stimulation of graphite precipitation during solidification, and due to its power as a graphitizing element (Onsoien and Skaland, 2001), its content was decided to be a factor in this study. Table 6 provides the chemistry for the SiC alloy added.

As for the metallographic characterization of the material, "slabs" were cut from the central zone of each cube, coinciding with the location of the highest value of the surface-to-volume ratio in the solid. Samples for the metallographic analysis were subsequently obtained from these slabs. Each slab was divided into 3 parts to identify the top, middle, and bottom zones. Eight metallographic samples were obtained from each of these three parts. Figure 1 shows the dimensions of the slabs in the cube and the zones from which the metallographic samples were taken. The analysis was carried out

TABLE 3. Objective and resulting compositions expressed in weight percent for each individual experiment

	Objective compositions					Resulting compositions				
No.	**%C**	**%Si**	**%Mn**	**%P**	**%Mg**	**%C**	**%Si**	**%Mn**	**%P**	**%Mg**
1	3.64	2	0.1	0.02	0.04	3.6	2	0.1	0.02	0.04
2	3.85	2	0.1	0.04	0.04	3.8	2	0.1	0.02	0.04
3	3.85	2	0.3	0.02	0.04	3.86	2	0.3	0.02	0.03
4	3.64	2	0.3	0.04	0.04	3.6	2.2	0.3	0.04	0.04
5	3.85	2	0.1	0.02	0.04	3.8	1.9	0.1	0.02	0.04
6	3.64	2	0.1	0.04	0.04	3.68	2.1	0.1	0.04	0.03
7	3.64	2	0.3	0.02	0.04	3.6	2	0.3	0.02	0.04
8	3.85	2	0.3	0.04	0.04	3.83	2.1	0.3	0.04	0.03
9	3.64	2	0.1	0.02	0.04	3.66	2	0.1	0.02	0.04
10	3.85	2	0.1	0.04	0.04	3.82	2	0.1	0.04	0.03
11	3.85	2	0.3	0.02	0.04	3.8	2	0.3	0.02	0.04
12	3.64	2	0.3	0.04	0.04	3.63	2.2	0.3	0.04	0.03
13	3.85	2	0.1	0.02	0.04	3.83	2	0.1	0.02	0.04
14	3.64	2	0.1	0.04	0.04	3.6	2	0.1	0.04	0.04
15	3.64	2	0.3	0.02	0.04	3.65	2.1	0.3	0.02	0.03
16	3.85	2	0.3	0.04	0.04	3.8	2	0.3	0.04	0.04

TABLE 4. Chemical composition of nodulizing alloys at each level expressed in weight percent (Factor "G" of the DOE matrix)

(a) Nodulizers at Level −1						
Nodulizer −1	**%Ce**	**%Mn**	**%Mg**	**%Al**	**%Si**	**Kg/T**
FeSiMg 1	1	—	5.5	1.2	44	4
FeSiMg 2	—	—	9	1.2	45	6
FeSiMg 3	—	0.3	—	0.12	72	2
(b) Nodulizers at Level +1						
Nodulizer +1	**%Ca**	**%La**	**%Mg**	**%Al**	**%Si**	**Kg/T**
La	0.55	0.34	5.69	0.38	45.3	6
FeSiMg 2	—	—	9	1.2	45	4

TABLE 5. Chemical composition expressed in weight percent of the post-inoculation alloys used in the study (Factor "F" of the DOE matrix)

Post-inoculants	**%Zr**	**%Mn**	**%Al**	**%Ca**	**%Si**	**Kg/T**
Post-Inoc.−1	—	—	3.9	1.9	74	2
Post-Inoc.+1	1.7	0.27	1.3	2.6	72	2

TABLE 6. Chemical composition expressed in weight percent of sic used in the study (Factor "C" of the DOE matrix)

SiC	**%Si**	**%C**	**Kg/T**
Level –1	72	0.3	3
Level +1	—	—	—

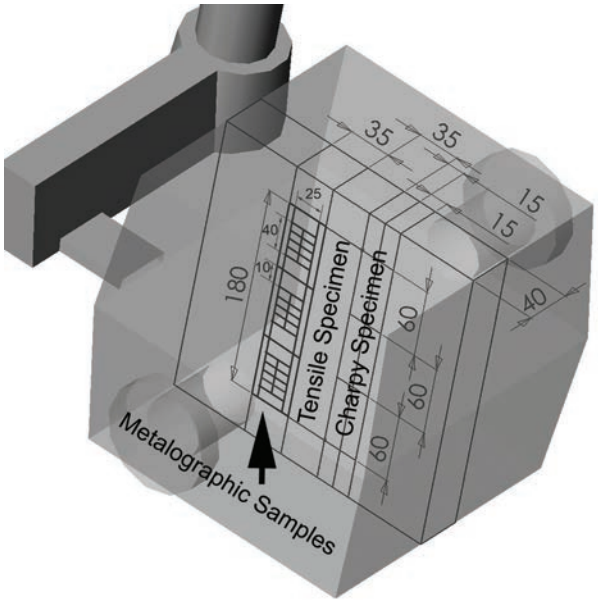

FIGURE 1. Location of the analyzed metallographic samples (see arrow) corresponding to the slab closer to the gating system in the cast cubes.

on micrographs recorded with a frame grabber and the quantitative characterization of the microstructure was conducted using the Image-Pro Plus 5.0 image analysis software and its Materials Pro module. The degree of "spheroidicity" of primary graphite was evaluated by a "roundness" parameter (Magenreuter *et al.*, 2008), defined as $\frac{[\text{perimeter}]^2}{4\pi(\text{area})}$.

This parameter defines the perfect nodule as one whose "roundness" falls within the (1–1.4) range, which happens to be the inverse for roundness provided by ASTM E2567-11 (2011), but leading to similar results.

3. RESULTS AND DISCUSSION

3.1. Statistical analysis

Table 7 shows the mean results for the volume fraction of pearlite, the volume fraction of graphite and the percentage of spheroidal graphite. The table also shows the effects obtained by applying Yates' algorithm (Johnson, 1997).

Figure 2 shows the representation of the factors on normal probability plot (Montgomery and Runger, 1996), illustrating in detail those factors that have a significant effect on the volume fraction of pearlite. The type of nodulizer employed and the Mn content are found to have a significant effect: the nodulizer employed at level –1, without lanthanum, and that of the Mn content at level +1 (0.3%-wt.) promote the presence of pearlite.

Figure 3 shows the representation of the factors on normal probability graph, illustrating in detail those factors having a significant effect on the volume fraction of primary graphite. In this case, the type of nodulizer, the Mn content, AC+BE+DG interactions and lastly AE+BC+DF interactions were found to have a significant effect (Johnson, 1997) on the mean volume fraction of graphite. The type of nodulizer without lanthanum acts as a graphitizing element compared to the one with a trace of lanthanum. Also, low Mn contents in the melt favour graphite formation, which seems logical as it is a carbide forming element. Tables 8 and 9 show the combined

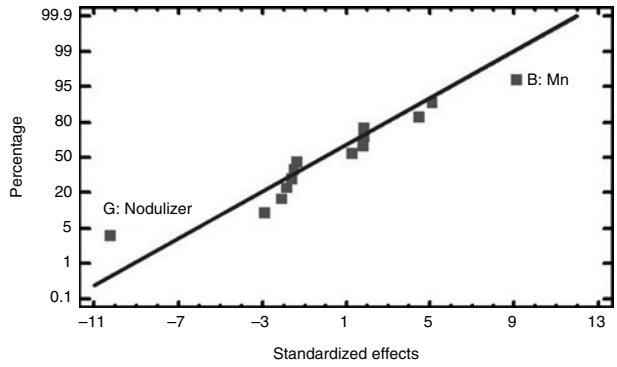

FIGURE 2. Normal Probability Plot for the mean volume fraction of pearlite.

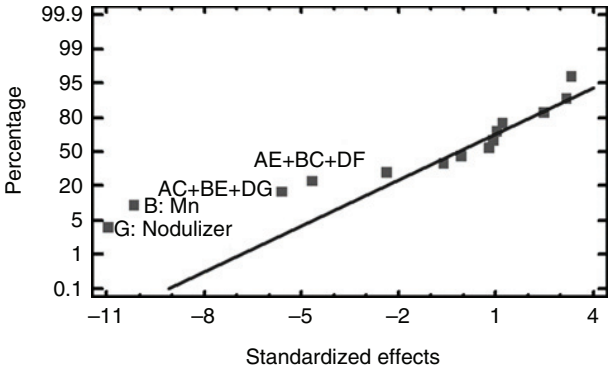

FIGURE 3. Normal Probability Plot for the mean volume fraction of graphite.

TABLE 7. Results obtained for the volume fraction of pearlite, primary graphite and percentage of spheroidal graphite

Test N°	Pearlite (% vol.)	effect	Graphite (% vol.)	effect	% spheroidal graphite	effect	
1	14.8	14.03	14.5	13.73	62	55.12	Mean
2	5.8	1.81	12.2	0.32	49	0.25	A
3	24.8	11.59	13.21	−2.72	53	−6.25	B
4	5.9	−2.31	13.6	0.85	46	−2.25	AB
5	2.5	−1.81	15.0	0.27	65	5.00	C
6	9.7	−3.01	16.0	−1.50	61	−3.50	AC
7	20.2	5.91	9.9	−1.25	48	−0.5	BC
8	21.3	−2.14	12.7	−0.02	64	−2.00	E
9	4.4	1.81	13.2	0.67	45	−1.75	D
10	23.4	6.71	17.4	−0.16	66	2.25	AD
11	6.1	1.74	9.8	−0.64	43	0.25	BD
12	34.3	1.69	14.8	−0.27	57	−8.75	ABD
13	3.0	−2.41	18.7	0.24	56	−2.00	CD
14	2.3	−12.06	13.6	−2.94	62	−11.50	G
15	29.2	1.11	14.2	0.89	68	0.00	F
16	16.8	−3.09	10.7	0.21	37	−5.50	AF

TABLE 8. Interactions AC+BE+DG with a significant effect on the volume fraction of primary graphite

		C				E				G	
AC+BE+DG		−1	1	AC+**BE**+DG		−1	1	AC+BE+**DG**		−1	1
A	−1	12.68	14.45	**B**	−1	14.34	15.82	**D**	−1	14.11	12.67
	1	14.50	13.27		1	13.13	11.6		1	16.28	11.84

TABLE 9. Interactions AE+BC+DF with a significant effect on the volume fraction of primary graphite

		E				C				F	
AE+BC+DF		−1	1	AE+**BC**+DF		−1	1	AE+BC+**DF**		−1	1
A	−1	12.95	14.18	**B**	−1	14.32	15.84	**D**	−1	12.32	14.46
	1	14.52	13.25		1	12.85	11.88		1	14.24	13.88

effect between pairs of factors of the aforementioned interactions. This allows the determination of combinations of two of those factors that provide the best results. Note that interaction DG could "skew" the significant effect of interactions AC+BE+DG, as high casting temperatures favour metastable solidification and could possibly promote the presence of solidification micro-shrinkages in segregated zones. These micro-cavities may "confuse" the image analyzer with graphite thus leading to misleading results (Pedersen and Tiedje, 2008).

Figure 4 shows an example of these micro-cavities, obtained in test No. 15. This effect could generate error as it erroneously increases the volume fraction of graphite in nital etched samples, while at the same time reduces the fraction of spheroidal graphite in those tests employing the nodulizer without any lanthanum (level +1). This is so due to the fact that low bearing La nodulizers promote the presence of pearlite in the colonies of which these micro-shrinkages appear. It should be noted, however, that the "whitening" effect of Mn is reduced with low level carbon equivalents (4.3%-wt.). As to the effect of interactions AE+BC+DF, a low content of Mn in combination with pre-inoculation of the molten iron with SiC, is found to promote and increase the volume fraction of precipitated graphite.

Figure 5 shows the representation of the factors on a normal probability plot, featuring those with a significant effect on the volume fraction of graphite presenting a roundness factor between 1 and 1.4 (which is considered to be quasi-spherical in this study). The type of nodulizer, the content of Mn, pre-inoculation of the ladle with SiC and AF+BG+DE interactions, are all found to have a significant effect. Hence, in order to increase the percentage of spheroidal graphite, it is necessary to use the nodulizer without lanthanum (level −1), scrap with a low content of Mn (level −1), and minimizing the SiC added as Si promotes the flake shape of graphite. Table 10 enables the selection of the most suitable combination of pairs from among the

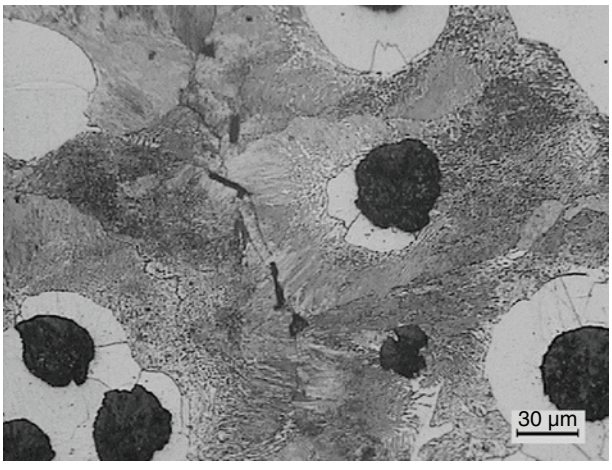

FIGURE 4. Micro-shrinkage porosity located in a pearlite aggregate.

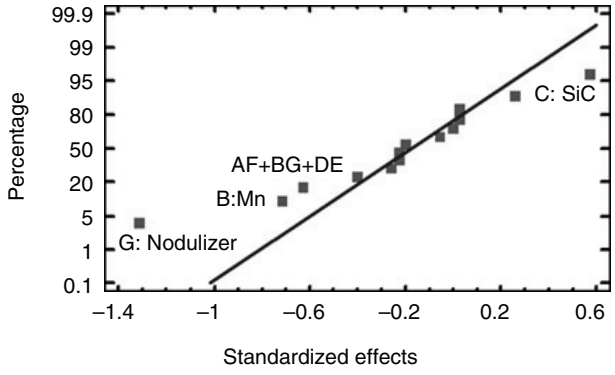

FIGURE 5. Normal Probability Plot for the mean fraction of spheroidal graphite.

Table 10. Interactions AF+BG+DE with a significant effect on the percentage of primary spheroidal graphite

		F				G				E	
AF+BG+DE		−1	1	AF+**BG**+DE		−1	1	AF+BG+**DE**		−1	1
A	−1	52.25	57.75	**B**	−1	61.25	55.25	**D**	−1	54.25	57.75
	1	58.00	52.50		1	60.50	43.50		1	58.00	50.50

design factors to optimize the effect of confusing AF+BG+DE interactions. It can thus be seen, for example, that it would be advisable to use scrap with low Mn contents (level −1) when using the nodulizer with traces of lanthanum (level +1).

3.2. Light optical microscopy

Figure 6 shows a representative micrograph for each of the 16 experiments, after etching the as-polished samples with 4% Nital (Radzikowska, 2005). These were obtained from equivalent zones in each slab.

3.3. Application of results

To corroborate the statistical results obtained from the Design of Experiments, a new cube was melted with Factors B, C, and G placed at their −1 levels. The metallographic characterization was performed as described in Section 2, Material and Methods. Furthermore, to verify that the mechanical properties obtained met the required specifications, a tensile specimen and three Charpy specimens were machined from the cube. Figure 1 shows the areas from which the necessary material for machining these specimens was obtained. The tensile specimen had a round resistant cross-section of 14 mm in diameter, the gauge length to measure elongation was 70 mm. The Charpy specimens had a length of 55 mm and a square cross-section of 10 mm each side. A 45° notch with a depth of 2 mm was machined at the centre point of the specimen. The tensile test was carried out as per the ISO 6892:1984 standard and the Charpy test, in compliance with the ISO 148:1983 standard. Table 11 shows all the manufacturing parameters of this cube and the results obtained. It should be noted that the percentage of perlite did not reach 2% and that the fraction of graphite with a spheroidal morphology exceeded

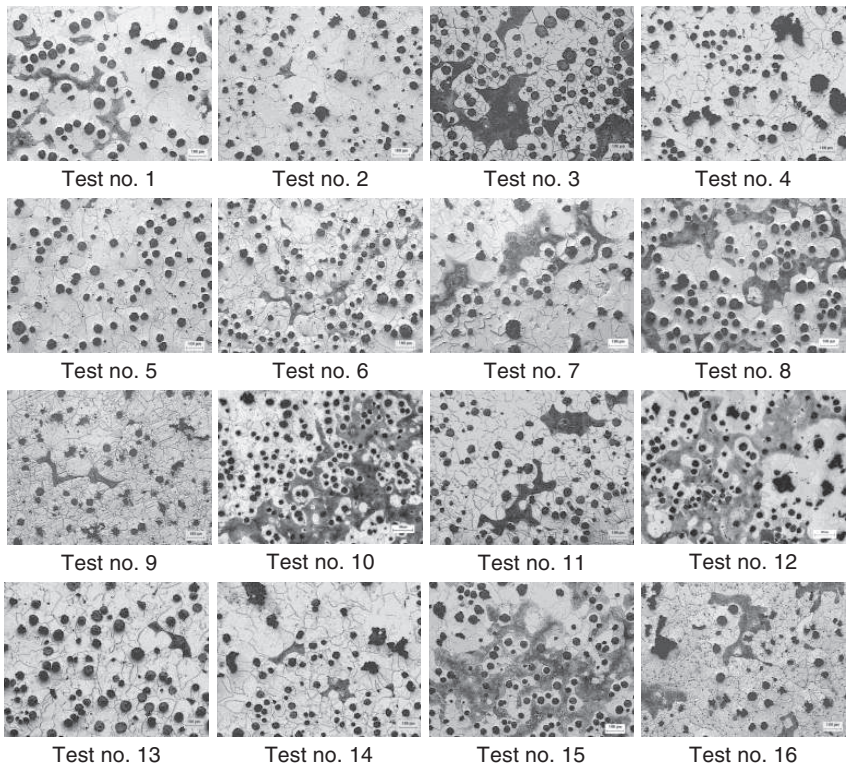

Figure 6. Representative micrographs from metallographic samples in each of the 16 experiments (etched with 4% nital).

TABLE 11. Parameters of the cube manufactured to corroborate the results of the Design of Experiments

(a) Levels of the factors of the matrix of experiments

A	B	C	D	E	F	G
–1	–1	+1	+1	–1	–1	–1

(b) Manufacturing parameters

Chemical Parameters					Non-chemical Parameters		
%C	%Si	%Mn	%P	%Mg	Casting Temperature	Nodulizer	Post-inoculant
3.62	2.1	0.1	0.02	0.04	1360 °C	–1	–1

(c) Results

Pearlite (%vol.)	Graphite (%vol.)	% spheroidal graphite	Yield Strength (MPa)	Tensile Strength (MPa)	Elongation (%)	Charpy Test (J)
1.98	16.62	68.8	247.11	387.25	18.75	11.8

Yield Strength calculated as $R_{p0.2\%}$
Charpy test performed on notched specimen V2, to −20 °C.
Charpy Test: Average value of 3 tests

68%. The results obtained from the mechanical tests exceeded the minimum required values.

4. CONCLUSIONS

- The use of nodulizers with trace levels of lanthanum for the manufacture of spheroidal graphite in ductile cast irons with a ferritic matrix favours the reduction of pearlite volume fraction. However, these nodulizers decrease the fraction of spheroidal graphite.
- Pre-inoculating with SiC and the use of scrap with relatively high Mn content were also found to have a negative effect on the spherical morphology of the graphite. Moreover, the use of scrap with a Mn content as high as 0.3%-wt., leads to an increase in the volume fraction of pearlite. It should be noted that this "whitening" effect of Mn is reduced with low carbon equivalents in the order of 4.3%-wt.

REFERENCES

Asenjo, I., Larrañaga, P., Garay, J., Sertucha, J. (2011). Influence of the chemical composition of different steel scraps on the mechanical properties of ductile iron. *Rev. Metal.* 47 (4), 307–318. https://doi.org/10.3989/revmetalm.1044.

Asensio-Lozano, J., Álvarez-Antolín, J.F. (2007). Application of Fractional Design of Experiments to the Optimisation of the Hardness and Microstructure of Duplex Cast Rolls. *Prakt. Metallogr.-Pract. Metallogr.* 44 (11), 503–522. https://doi.org/10.3139/147.100360.

Asensio-Lozano, J., Álvarez-Antolín, J.F., Vander Voort, G.F. (2008). Identification and quantification of active manufacturing factors for graphite formation in centrifugally cast Nihard cast irons. *J. Mater. Process. Tech.* 206 (1–3), 202–215. https://doi.org/10.1016/j.jmatprotec.2007.12.015.

ASTM E2567-11 (2011). Standard Test Method for Determining Nodularity And Nodule Count In Ductile Iron Using Image Analysis, ASTM International, West Conshohocken, PA.

Bockus, S., Zaldarys, G. (2010). Production of Ductile Iron Castings with Different Matrix Structure. *Mater. Sci.-Medzg.* 16 (4), 307–310. http://internet.ktu.lt/lt/mokslas/zurnalai/medz/pdf/medz0-103/05%20Metals...(pp.307-310).pdf.

Box, G., Hunter, J., Hunter, W. (2005). *Statistics for Experimenters*. John Wiley & Sons, Inc., New York, USA.

Geier, G.F., Bauer, W., McKay, B.J., Schumacher, P. (2005). Microstructure transition from lamellar to compacted graphite using different modification agents. *Mat. Sci. Eng. A-Struct.* 413–414, 339–345. https://doi.org/10.1016/j.msea.2005.08.159.

Guzel, E., Yuksel, C., Bayrak, Y., Sen, O., Ekerim, A. (2014). Effect of section thickness on the microstructure and hardness of ductile cast iron. *Mater. Test.* 56 (4), 285–288. https://doi.org/10.3139/120.110558.

Han, S.Y., Sohn, S.S., Shin, S.Y., Lee, S., Suh, Y.C. (2013). In Situ fracture observation and fracture toughness analysis of pearlitic graphite cast irons with different nodularity. *Met. Mater. Int.* 19 (4), 673–682. https://doi.org/10.1007/s12540-013-4006-6.

Johnson, R.A. (1997). *Probabilidad y Estadística para Ingenieros*. Prentice-Hall Hispanoamérica, México.

Lacaze, J., Sertucha, J., Larrañaga, P., Suárez, R. (2016). Statistical study to determine the effect of carbon, silicon, nickel and other alloying elements on the mechanical properties of as-cast ferritic ductile irons. *Rev. Metal.* 52 (2), e070. https://doi.org/10.3989/revmetalm.070.

Magenreuter, T., Velichko, A., Mücklich, F. (2008). The dependence of the shape parameters roundness and compactness of various graphite morphologies on magnification. *Prakt. Metallogr.- Pract. Metallogr.* 45 (2), 53–71. https://doi.org/10.3139/147.100371.

Montgomery, D.C., Runger, G.C. (1996). *Probabilidad y Estadística aplicada a la Ingeniería*. Mc Graw-Hill, México.

Mottitschka, T., Pusch, G., Biermann, H., Zybell, L., Kuna, M. (2012). Influence of graphite spherical size on fatigue behaviour and fracture toughness of ductile cast iron EN-GJS-400-18LT. *Int. J. Mater. Res.* 103 (1), 87–96. https://doi.org/10.3139/146.110636.

Onsoien, M.I., Skaland, T., Grong, O. (1999). Mechanisms of graphite formation in ductile cast iron containing cerium and lanthanum. *Int. J. Cast. Metal. Res.* 11 (5), 319–324. https://doi.org/10.1080/13640461.1999.11819293.

Onsoien, M.I., Skaland, T. (2001). Preconditioning of Gray Iron Melts using Ferrosilicon or Silicon Carbide. 105th Casting Congress, American Foundry Society (AFS), Dallas, USA.

Pan, Y.N., Lin, C.C., Chang, R.M. (2012). Assessments of relationship between microstructures and mechanical properties for heavy section ductile cast irons. *Int. J. Mater. Res.* 25 (5), 301–306. https://doi.org/10.1179/1743133612Y.0000000027.

Pedersen, K.M, Tiedje, N.S. (2008). Graphite nodule count and size distribution in thin-walled ductile cast iron. *Mater. Charact.* 59 (8), 1111–1121. https://doi.org/10.1016/j.matchar.2007.09.001.

Pedersen, K.M., Tiedje, N.S. (2009). Influence of rare earths on shrinkage porosity in thin walled ductile cast iron. *Int. J. Cast. Metal. Res*. 22 (1–4), 302–305. https://doi.org/10.1179/136404609x367830.

Prat, A., Tort-Martorell, X., Grima, P., Pozueta, L. (1997). *Métodos estadísticos control y mejora de la calidad*. Ediciones UPC, Barcelona, España.

Radzikowska, J.M. (2005). Effect of specimen preparation on evaluation of cast iron microstructures. *Mater. Charact.* 54 (4–5), 287–304. https://doi.org/10.1016/j.matchar.2004.08.019.

Sheikh, M.A., Iqbal, J. (2007). Effect of lanthanum on nodule count and nodularity of ductile iron. *J. Rare Earths* 25 (5), 533–536. https://doi.org/10.1016/S1002-0721(07)60557-2.

Shiraki, N., Watanabe, T., Kanno, T. (2015). Relationship between Fatigue Limit and Defect Size in Spheroidal Graphite Cast Iron with Different Graphite Spheroidization Ratios and Microstructures. *Mater. Trans*. 56 (12), 2010–2016. https://doi.org/10.2320/matertrans.F-M2015826.

Shiraki, N., Usui, Y., Kanno, T. (2016). Effects of Number of Graphite Nodules on Fatigue Limit and Fracture Origins in Heavy Section Spheroidal Graphite Cast Iron. *Mater. Trans.* 57 (3), 379–384. https://doi.org/10.2320/matertrans.F-M2015841.

Skjegstad, N.T., Skaland, T. (1996). Inoculation of Grey and Ductile Iron. Proceedings of Bombay Foundry Congress, Bombay, India, pp. 1–23.

Soivio, K., Elmquist, L. (2013). Influence of inoculation on shrinkage defects in spheroidal graphite cast iron. *Int. J. Cast. Metal Res*. 26 (4), 220–227. https://doi.org/10.1179/1743133613Y.0000000057.